

Multi-hop quantum teleportation based on HSES via GHZ-like states

She-Xiang Jiang(蒋社想), Xiao-Long Wei(韦晓龙), Jin-Huan Li(李金欢), and Shuai-Shuai Li(李帅帅)

Citation: Chin. Phys. B, 2025, 34 (**1**): 010302. DOI: 10.1088/1674-1056/ad8db0
Journal homepage: http://cpb.iphy.ac.cn; http://iopscience.iop.org/cpb

What follows is a list of articles you may be interested in

Machine-learning-assisted efficient reconstruction of the quantum states generated from the Sagnac polarization-entangled photon source

Menghui Mao(毛梦辉), Wei Zhou(周唯), Xinhui Li(李新慧), Ran Yang(杨然), Yan-Xiao Gong(龚彦晓), and Shi-Ning Zhu(祝世宁)
Chin. Phys. B, 2024, 33 (**8**): 080301. DOI: 10.1088/1674-1056/ad51f7

Degenerate polarization entangled photon source based on a single Ti-diffusion lithium niobate waveguide in a polarization Sagnac interferometer

Yu Sun(孙宇), Chang-Wei Sun(孙昌伟), Wei Zhou(周唯), Ran Yang(杨然), Jia-Chen Duan(端家晨), Yan-Xiao Gong(龚彦晓), Ping Xu(徐平), and Shi-Ning Zhu(祝世宁)
Chin. Phys. B, 2023, 32 (**8**): 080308. DOI: 10.1088/1674-1056/acd8b3

Hierarchical simultaneous entanglement swapping for multi-hop quantum communication based on multi-particle entangled states

Guang Yang(杨光, Lei Xing(邢磊), Min Nie(聂敏), Yuan-Hua Liu(刘原华), and Mei-Ling Zhang(张美玲)
Chin. Phys. B, 2021, 30 (**3**): 030301. DOI: 10.1088/1674-1056/abcf3d

Anonymous voting for multi-dimensional CV quantum system

Rong-Hua Shi(施荣华), Yi Xiao(肖伊), Jin-Jing Shi(石金晶), Ying Guo(郭迎), Moon-Ho Lee
Chin. Phys. B, 2016, 25 (**6**): 060301. DOI: 10.1088/1674-1056/25/6/060301

Controlled mutual quantum entity authentication using entanglement swapping

Min-Sung Kang, Chang-Ho Hong, Jino Heo, Jong-In Lim, Hyung-Jin Yang
Chin. Phys. B, 2015, 24 (**9**): 090306. DOI: 10.1088/1674-1056/24/9/090306

SPECIAL TOPIC — Quantum communication and quantum network

Multi-hop quantum teleportation based on HSES via GHZ-like states

She-Xiang Jiang(蒋社想), Xiao-Long Wei(韦晓龙)†, Jin-Huan Li(李金欢), and Shuai-Shuai Li(李帅帅)

School of Computer Science and Engineering, Anhui University of Science and Technology, Huainan 232001, *China*

(Received 26 July 2024; revised manuscript received 12 October 2024; accepted manuscript online 1 November 2024)

Implementing quantum wireless multi-hop network communication is essential to improve the global quantum network system. In this paper, we employ eight-level GHZ states as quantum channels to realize multi-hop quantum communication, and utilize the logical relationship between the measurements of each node to derive the unitary operation performed by the end node. The hierarchical simultaneous entanglement switching (HSES) method is adopted, resulting in a significant reduction in the consumption of classical information compared to multi-hop quantum teleportation (QT) based on general simultaneous entanglement switching (SES). In addition, the proposed protocol is simulated on the IBM Quantum Experiment platform (IBM QE). Then, the data obtained from the experiment are analyzed using quantum state tomography, which verifies the protocol's good fidelity and accuracy. Finally, by calculating fidelity, we analyze the impact of four different types of noise (phase-damping, amplitude-damping, phase-flip and bit-flip) in this protocol.

Keywords: multi-hop quantum teleportation, GHZ-like state, hierarchical simultaneous entanglement swapping, IBM Quantum Experiment platform, quantum state tomography

PACS: 03.67.Hk, 03.67.Pp, 03.67.–a

DOI: 10.1088/1674-1056/ad8db0 **CSTR:** 32038.14.CPB.ad8db0

1. Introduction

Quantum teleportation (QT) is one of the most important technologies in quantum communication. It is a technique utilizing quantum entanglement and classical communication to transfer quantum states from one location to another. Since Bennett *et al.*[1] proposed the first quantum teleportation protocol using the Einstein–Podolsky–Rosen (EPR) state as a quantum channel in 1993, subsequent literature[2] has proved the validity of this work through experiments. Since then, this novel technique has become a research hotspot in quantum communication. Subsequently, various quantum teleportation schemes based on different multiparticle entangled states have been proposed, including those using Bell states,[3,4] GHZ states,[5–7] GHZ-like states[8–10] and W states.[11]

However, most of these protocols involve point-to-point communication, which is unsuitable for long-distance quantum information transmission. To address this issue, Briegel *et al.*[12] initially proposed the concept of quantum repeaters, leading to the subsequent development of various protocols based on this idea. Then, a quantum routing mechanism within a hierarchical network architecture was proposed for wirelessly transmitting a quantum state from one party to another,[13] even when they do not directly share an entangled state between them. Therefore, long-distance transmission of quantum information requires multiple intermediate nodes. Utilizing entanglement between adjacent nodes, multi-hop quantum teleportation has emerged as a key research area in quantum communication. In recent years, various multi-hop quantum teleportation schemes have been proposed. Wang *et al.*[14] proposed a multi-hop teleportation based on a simultaneous swapping scheme (SES), utilizing arbitrary Bell states as a quantum channel, which enables the possibility of long-distance and low-latency communication. Subsequently, using the SES scheme, different multi-hop protocols were designed using various entangled states, such as the bidirectional multi-hop teleportation protocol using GHZ–Bell states[15] and GHZ states.[16] Multi-hop protocols also determine the quantum channel based on the parity of the number of hops, such as GHZ–Bell states,[17] GHZ–class and Bell states.[18] However, in SES, each intermediate node is required to send its measurement results and the type of entangled state to the target node. This leads to high classical communication costs due to the continuous forwarding of classical information in the channel. To address this issue, Yang *et al.*[19] introduced the hierarchical simultaneous entanglement swapping (HSES) scheme, effectively reducing the classical communication cost.

Inspired by the ideas presented in the literature,[19] in this paper we propose a multi-hop teleportation scheme based on simultaneous entanglement switching, utilizing GHZ-like states as a quantum channel. The deployment of GHZ-like states, because they have more variations than Bell states and neighboring nodes on the path, will most likely not share the same entangled state, thus improving the security of the quantum channel. Furthermore, the unitary operator for the target states is determined using logical operators. In addition, we conduct experiments on one-hop QT and two-hop QT proto-

†Corresponding author. E-mail: 461242289@qq.com

© 2025 Chinese Physical Society and IOP Publishing Ltd. All rights, including for text and data mining, AI training, and similar technologies, are reserved.

cols on the IBM Quantum Experience (QE) platform, analyze the results, and compare the theoretical and experimental density matrices using quantum state tomography. This is followed by calculating the fidelity of the scheme to verify the accuracy of the transmitted quantum states.

In recent years, some researchers have investigated using GHZ-like states as a quantum channel.[8–10,18] The most significant property of GHZ-like states is that manipulating any of one of the three qubits results in the entanglement of the other two. GHZ-like states consist of a Bell state and a single-qubit quantum state, as shown by the following equation:

$$\begin{aligned}
|\xi_{000}\rangle_{123} &= \frac{1}{\sqrt{2}}(|\beta_{00}\rangle|0\rangle+|\beta_{01}\rangle|1\rangle)_{123},\\
|\xi_{001}\rangle_{123} &= \frac{1}{\sqrt{2}}(|\beta_{10}\rangle|0\rangle+|\beta_{11}\rangle|1\rangle)_{123},\\
|\xi_{010}\rangle_{123} &= \frac{1}{\sqrt{2}}(|\beta_{00}\rangle|0\rangle-|\beta_{01}\rangle|1\rangle)_{123},\\
|\xi_{011}\rangle_{123} &= \frac{1}{\sqrt{2}}(|\beta_{10}\rangle|0\rangle-|\beta_{11}\rangle|1\rangle)_{123},\\
|\xi_{100}\rangle_{123} &= \frac{1}{\sqrt{2}}(|\beta_{00}\rangle|1\rangle+|\beta_{01}\rangle|0\rangle)_{123},\\
|\xi_{101}\rangle_{123} &= \frac{1}{\sqrt{2}}(|\beta_{10}\rangle|1\rangle+|\beta_{11}\rangle|0\rangle)_{123},\\
|\xi_{110}\rangle_{123} &= \frac{1}{\sqrt{2}}(|\beta_{00}\rangle|1\rangle-|\beta_{01}\rangle|0\rangle)_{123},\\
|\xi_{111}\rangle_{123} &= \frac{1}{\sqrt{2}}(|\beta_{10}\rangle|1\rangle-|\beta_{11}\rangle|0\rangle)_{123},
\end{aligned} \tag{1}$$

where $|\beta\rangle_{ij}$ represents Bell states, as shown by the following equation:

$$\begin{aligned}
|\beta\rangle_{00} &= \frac{1}{\sqrt{2}}(|00\rangle+|11\rangle), \quad |\beta\rangle_{01} = \frac{1}{\sqrt{2}}(|01\rangle+|10\rangle),\\
|\beta\rangle_{10} &= \frac{1}{\sqrt{2}}(|00\rangle-|11\rangle), \quad |\beta\rangle_{11} = \frac{1}{\sqrt{2}}(|01\rangle-|10\rangle).
\end{aligned} \tag{2}$$

The rest of the paper is organized as follows. Section 2 introduces one-hop, two-hop and multi-hop QT, respectively. Section 3 presents a multi-hop QT scheme based on arbitrary GHZ-class states. Section 4 describes a multi-hop QT scheme based on the HSES scheme. Section 5 provides an experimental analysis of our multi-hop QT scheme using the IBM QE platform. Section 6 analyzes the impact of four common types of noise (phase-damping, amplitude-damping, phase-flip and bit-flip) on this protocol. Section 7 discusses the communication delay and classical resource consumption of the proposed schemes, comparing it with other schemes in terms of classical resource usage. Finally, the summary of our work is given in Section 8.

2. Multi-hop QT with GHZ-like state

2.1. One-hop QT with GHZ-like state

Consider two nodes in a one-hop quantum teleportation, one belonging to Alice and the other to Bob. They share an entangled state between them. Alice now wants to send particle $|\psi\rangle_0 = (\alpha|0\rangle+\beta|1\rangle)_0$ to Bob, where α and β are complex numbers satisfying $|\alpha|^2+|\beta|^2=1$. Suppose Alice prepares a GHZ-like state and assigns particle 3 to Bob, as illustrated in the following equation:

$$|\xi_{000}\rangle_{123} = \frac{1}{2}(|000\rangle+|110\rangle+|011\rangle+|101\rangle)_{123}. \tag{3}$$

The whole system can be represented by the following equation:

$$|\Lambda\rangle_{0123} = |\psi\rangle_0 \otimes |\xi_{000}\rangle_{123}, \tag{4}$$

where particles 0, 1 and 2 belong to Alice, and particle 3 belongs to Bob.

Figure 1 illustrates the basic quantum circuit for one-hop teleportation. For the source node, Alice performs a controlled-NOT (CNOT) gate on her particles (0,1), where 0 is the control bit. Then, Alice performs the Hadamard gate operation on particle 0. The whole system can be converted into

$$\begin{aligned}
|\Lambda\rangle_{0123} = \frac{1}{2\sqrt{2}}(&|000\rangle_{012}|\psi\rangle_3+|001\rangle_{012}X|\psi\rangle_3\\
&+|010\rangle_{012}X|\psi\rangle_3+|011\rangle_{012}X|\psi\rangle_3\\
&+|100\rangle_{012}Z|\psi\rangle_3+|101\rangle_{012}XZ|\psi\rangle_3\\
&+|110\rangle_{012}XZ|\psi\rangle_3+|111\rangle_{012}Z|\psi\rangle_3).
\end{aligned} \tag{5}$$

Alice performs a projection measurement of her particle (0,1,2) using a three-bit measurement basis $|ijk\rangle$ ($ijk\in\{0,1\}$). Here, the outcomes of these measurements are denoted as (R_1, R_2) and R_0, respectively. The measurement results indicate that Bob's qubit can be transformed into one of the states $|\psi\rangle_3$, $X|\psi\rangle_3$, $Z|\psi\rangle_3$ and $XZ|\psi\rangle_3$. Once Bob receives the measurement results, he can apply the appropriate Pauli operator to convert particle 3 into the initial state $|\psi\rangle$. The relationship between the specific measurement results and the corresponding Pauli operator is shown in Table 1.

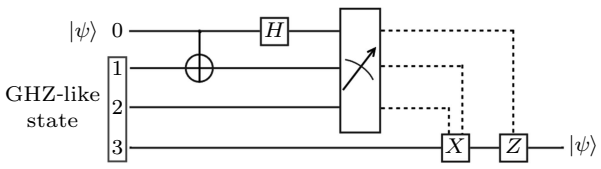


Fig. 1. One-hop QT quantum circuit.

Table 1. Relationship between each node measurement and the execution of the Pauli operator at the target node in a one-hop QT.

Measurement results R_0	Measurement results $R_1 \oplus R_2$	Pauli operators on particle 3
0	0	I
0	1	X
1	0	Z
1	1	ZX

2.2. Two-hop QT with GHZ-like state

In a multi-hop quantum network, the source and target nodes may not share the entangled state directly, so transferring quantum information via the entanglement of intermediate nodes is necessary. Two-hop QT is similar to one-hop QT but involves three nodes in the network, which are the source node, intermediate node and target node. The challenge is determining how the source node can transmit quantum information to the target node. Figure 2 shows the node distribution in a two-hop QT. Alice and Charlie each prepare a GHZ-like state. Alice assigns particle 3 to Charlie, Charlie assigns particle 6 to Bob, and the whole system is as follows:

$$\begin{aligned}|\Lambda\rangle_{0123456} &= |\psi\rangle_0 \otimes |\gamma\rangle_{123456} \\ &= |\psi\rangle_0 \otimes |\xi_{000}\rangle_{123} \otimes |\xi_{000}\rangle_{456}. \end{aligned} \tag{6}$$

Alice and Charlie perform CNOT gate operations on their particle pairs (0,1) and (3,4), respectively, where particles 0 and 3 are control bits, and then perform H gate operations on particles 0 and 3. The total state change is as follows:

$$\begin{aligned}|\Lambda\rangle_{0123456} = \frac{1}{8}[&(|000000\rangle + |000011\rangle + |011000\rangle \\ &+ |011011\rangle + |001010\rangle + |001001\rangle \\ &+ |010010\rangle + |010001\rangle + |100100\rangle \\ &+ |100111\rangle + |111100\rangle + |111111\rangle \\ &- |101110\rangle - |101101\rangle - |110110\rangle \\ &- |110101\rangle)_{012345}|\psi\rangle_6 \\ &+ (|000001\rangle + |000010\rangle + |011001\rangle \\ &+ |011010\rangle + |001011\rangle + |001000\rangle \\ &+ |010011\rangle + |010000\rangle + |100101\rangle \\ &+ |100110\rangle + |111101\rangle + |111110\rangle \\ &- |101111\rangle - |101100\rangle - |110111\rangle \\ &- |110100\rangle)_{012345}X|\psi\rangle_6 \\ &+ (|000100\rangle + |000111\rangle + |011100\rangle \\ &+ |011111\rangle - |001110\rangle - |001101\rangle \\ &- |010110\rangle - |010101\rangle + |100000\rangle \\ &+ |100011\rangle + |111000\rangle + |111011\rangle \\ &+ |101010\rangle + |101001\rangle + |110010\rangle \\ &+ |110001\rangle)_{012345}Z|\psi\rangle_6 \\ &+ (|000101\rangle + |000110\rangle + |011101\rangle \\ &+ |011110\rangle - |001111\rangle - |001100\rangle \\ &- |010111\rangle - |010100\rangle + |100001\rangle \\ &+ |100010\rangle + |111001\rangle + |111010\rangle \\ &+ |101011\rangle + |101000\rangle + |110011\rangle \\ &+ |110000\rangle)_{012345}ZX|\psi\rangle_6]. \end{aligned} \tag{7}$$

Alice and Charlie perform projection measurements on their own particles (0,1,2), (3,4,5) using a three-bit measurement basis $|ijk\rangle$, respectively. Here, the outcomes of these measurements are noted as (R_1, R_2), R_0, (R_4, R_5) and R_3, respectively. They then send the measurement results to Bob through the classical channel. By employing the results, Bob can reconstruct the initial state by applying the corresponding Pauli operators to particle 6. The details are presented in Table 2.

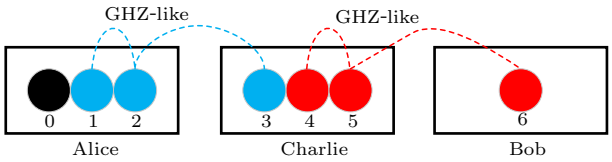


Fig. 2. Two-hop QT node distribution.

Table 2. Relationship between each node measurement and the execution of the Pauli operator at the target node in a one-hop QT.

Measurement results $R_0 \oplus R_3$	Measurement results $R_1 \oplus R_2 \oplus R_4 \oplus R_5$	Pauli operators on particle 6
0	0	I
0	1	X
1	0	Z
1	1	ZX

From Tables 1 and 2, the relationship between the measurements in one-hop QT and two-hop QT and the execution of the Pauli operator can be derived. The correlation between Bob's Pauli operations and the measurements for each group is deduced by introducing logical relations. For instance, in Table 2, if the logical expression algebraically is $\overline{R_0 \oplus R_3} \cdot R_1 \oplus R_2 \oplus R_4 \oplus R_5 = 1$, Bob can reconfigure the initial state of particle 6 using a logical gate X. The signals $\oplus$, $\cdot$, $-$ denote logical operators XOR, AND, NOT, respectively. The relationship between each set of logical algebraic expressions and the Pauli operator executed by the target node is recorded in Table 3.

Table 3. The relationship between logical algebraic expressions and the Pauli operator executed by the target node.

Logical algebra expression for one-hop	Logical algebra expression for two-hop	Pauli operators on destination particle
$\overline{R_0} \cdot \overline{R_1 \oplus R_2} = 1$	$\overline{R_0 \oplus R_3} \cdot \overline{R_1 \oplus R_2 \oplus R_4 \oplus R_5} = 1$	I
$\overline{R_0} \cdot R_1 \oplus R_2 = 1$	$\overline{R_0 \oplus R_3} \cdot R_1 \oplus R_2 \oplus R_4 \oplus R_5 = 1$	X
$R_0 \cdot \overline{R_1 \oplus R_2} = 1$	$R_0 \oplus R_3 \cdot \overline{R_1 \oplus R_2 \oplus R_4 \oplus R_5} = 1$	Z
$R_0 \cdot R_1 \oplus R_2 = 1$	$R_0 \oplus R_3 \cdot R_1 \oplus R_2 \oplus R_4 \oplus R_5 = 1$	ZX

2.3. Multi-hop QT with GHZ-like state

The one-hop QT and two-hop QT schemes described above can be extended to multi-hop QT. The scheme presented in the previous sections is generalized by transmitting an arbitrary single bit in a multi-hop quantum teleportation using a composite state of GHZ-like states as the channel. Assuming that there are n nodes in multi-hop QT, the first node N_0 as the sender can transmit to the end node N_{n-1} through $n-1$ hop communication. Thus, the whole system comprises $n-1$ intermediate nodes that prepare GHZ-like states to form a quantum channel for transmitting quantum information, as shown in Fig. 3.

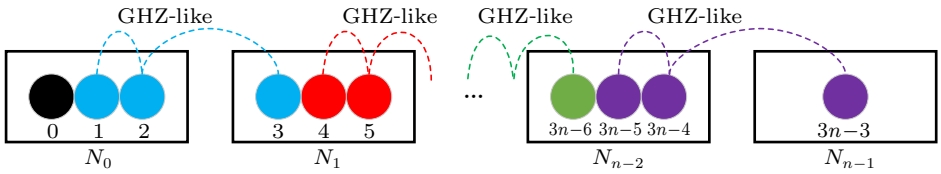


Fig. 3. Multi-hop QT node distribution.

Table 4. Relationship between each node measurement and the execution of the Pauli operator at the target node in a two-hop QT.

Measurement results R_0 to R_{3n-2}	Pauli operators on particle R_{3n-2}
$\overline{\oplus_{i=0}^{i=n-1} R_{3i}} \cdot \overline{\oplus_{i=0}^{i=n-1} R_{3i+1} \oplus R_{3i+2}} = 1$	I
$\overline{\oplus_{i=0}^{i=n-1} R_{3i}} \cdot \oplus_{i=0}^{i=n-1} R_{3i+1} \oplus R_{3i+2} = 1$	X
$\oplus_{i=0}^{i=n-1} R_{3i} \cdot \overline{\oplus_{i=0}^{i=n-1} R_{3i+1} \oplus R_{3i+2}} = 1$	Z
$\oplus_{i=0}^{i=n-1} R_{3i} \cdot \oplus_{i=0}^{i=n-1} R_{3i+1} \oplus R_{3i+2} = 1$	ZX

The whole system can be represented as

$$|\Lambda\rangle_{012\ldots3n-3} = |\psi\rangle_0 \otimes \left(\otimes_{i=0}^{i=n-2} |\xi_{000}\rangle\right)_{12\ldots3n-3}. \tag{8}$$

Each node, except the end node, assigns the third particle of its GHZ-like state to the subsequent node. Then, each node performs a CNOT gate on its first and second particles, where the first particle is the control bit, and performs an H gate operation on the first particle. Table 4 gives the relationship between each intermediate node's particle measurements and the target node's corresponding Pauli operation. The end node, N_{n-1}, can recover the target state by executing the corresponding Pauli operation in Table 4 according to the measurement results of the intermediate nodes.

3. General multi-hop QT with arbitrary GHZ-like states

In the scheme above, each intermediate node produces only one GHZ-like state $|\xi_{000}\rangle$, which means we use only one GHZ-like composite state for the quantum channel. However, in practical scenarios, the quantum channel can be a composite of these eight GHZ-like states $|\xi_{000}\rangle, |\xi_{001}\rangle, |\xi_{010}\rangle, |\xi_{011}\rangle, |\xi_{100}\rangle, |\xi_{101}\rangle, |\xi_{110}\rangle, |\xi_{111}\rangle$. To enhance the diversity of the quantum channel, the intermediate nodes are required to send the GHZ-like type and the measurement results to the end node since

$$\begin{aligned} |\xi_{000}\rangle &= Z_1 |\xi_{001}\rangle = Z_3 |\xi_{010}\rangle = Z_2 |\xi_{011}\rangle = X_3 |\xi_{100}\rangle \\ &= X_3 Z_1 |\xi_{101}\rangle = X_3 Z_3 |\xi_{110}\rangle = X_3 Z_2 |\xi_{111}\rangle. \end{aligned} \tag{9}$$

Table 5. Relationship between the target node performing the modified unitary operation and different types of GHZ-like states.

Mod 2 results of eight types of GHZ-class states	Pauli
00000000,00000011,00000101,00000110,00011001,00011010,00011100,00011111, 00101001,00101010,00101100,00101111,00110000,00110011,00110101,00110110, 01001001,01001010,01001100,01001111,01010000,01010011,01010101,01010110, 01100000,01100011,01100101,01100110,01111001,01111010,01111100,01111111, 10000000,10000011,10000101,10000110,10011001,10011010,10011100,10011111, 10101001,10101010,10101100,10101111,10110000,10110011,10110101,10110110, 11001001,11001010,11001100,11001111,11010000,11010011,11010101,11010110, 11100000,11100011,11100101,11100110,11111001,11111010,11111100,11111111	I
00001000,00001011,00001101,00001110,00010001,00010010,00010100,00010111, 00100001,0010010,00100100,00100111,00111000,00111011,00111101,00111110, 01000001,01000010,01000100,01000111,01011000,01011011,01011101,01011110, 01101000,01101011,01101101,01101110,01110001,01110010,01110100,01110111, 10001000,10001011,10001101,10001110,10010001,10010010,10010100,10010111, 10100001,10100010,10100100,10100111,10111000,10111011,10111101,10111110, 11000001,11000010,11000100,11000111,11011000,11011011,11011101,11011110, 11101000,11101011,11101101,11101110,11110001,11110010,11110100,11110111	X
00001001,00001010,00001100,00001111,00010000,00010011,00010101,00010110, 00100000,00100011,00100101,00100110,00111001,00111010,00111100,00111111, 01000000,01000011,01000101,01000110,01011001,01011010,01011100,01011111, 01101001,01101010,01101100,01101111,01110000,01110011,01110101,01110110, 10001001,10001010,10001100,10001111,10010000,10010011,10010101,10010110, 10100000,10100011,10100101,10100110,10111001,10111010,10111100,10111111, 11000000,11000011,11000101,11000110,11011001,11011010,11011100,11011111, 11101001,11101010,11101100,11101111,11110000,11110011,11110101,11110110	Z
00000001,00000010,00000100,00000111,00011000,00011011,00011101,00011110, 00101000,00101011,00101101,00101110,00110001,00110010,00110100,00110111, 01001000,01001011,01001101,01001110,01010001,01010010,01010100,01010111, 01100001,01100010,01100100,01100111,01111000,01111011,01111101,01111110, 10000001,10000010,10000100,10000111,10011000,10011011,10011101,10011110, 10101000,10101011,10101101,10101110,10110001,10110010,10110100,10110111, 11001000,11001011,11001101,11001110,11010001,11010010,11010100,11010111, 11100001,11100010,11100100,11100111,11111000,11111011,11111101,11111110	ZX

It can be shown that the final unitary operation at the end node is determined by the number of different types of GHZ-like states produced by all the intermediate nodes, irrespective of their order. Hence, the end nodes must count the number of these eight types of GHZ-like states and calculate the modified unitary operation, as shown in Table 5. The eight-bit sequence code in the table represents the result of mod 2 for the number of eight GHZ-like state types.

Taking the two jumps in the previous section as an example, assume that the types of the GHZ-like states prepared by Alice and Charlie are $|\xi_{010}\rangle$ and $|\xi_{101}\rangle$, respectively, the counts of $|\xi_{010}\rangle$, $|\xi_{101}\rangle$ mod 2 are 1 and 1, respectively, and the counts of the other GHZ-like states are 0. Therefore, we obtain the eight-bit sequence number 01001000. According to Table 5, we derive that the corresponding unitary operator is ZX. Bob obtains the basic unitary operator from Table 5 and the modified unitary operator from Table 5. The final unitary operator can be obtained by simply multiplying these two operators.

4. Multi-hop QT based on HSES

In traditional multi-hop QT, intermediate nodes not only send the measurement results but also the entanglement states shared with neighboring nodes, leading to significant classical resource wastage. To reduce the consumption of classical resources, our scheme employs hierarchical simultaneous entanglement swapping (HSES).[19] This approach is similar to the scheme described in the previous sections, but in HSES, the intermediate nodes on the quantum path are divided into segments according to the network size, as shown in Fig. 4, and the end node of each segment is indicated by gray color. A complete HSES process consists of the following steps.

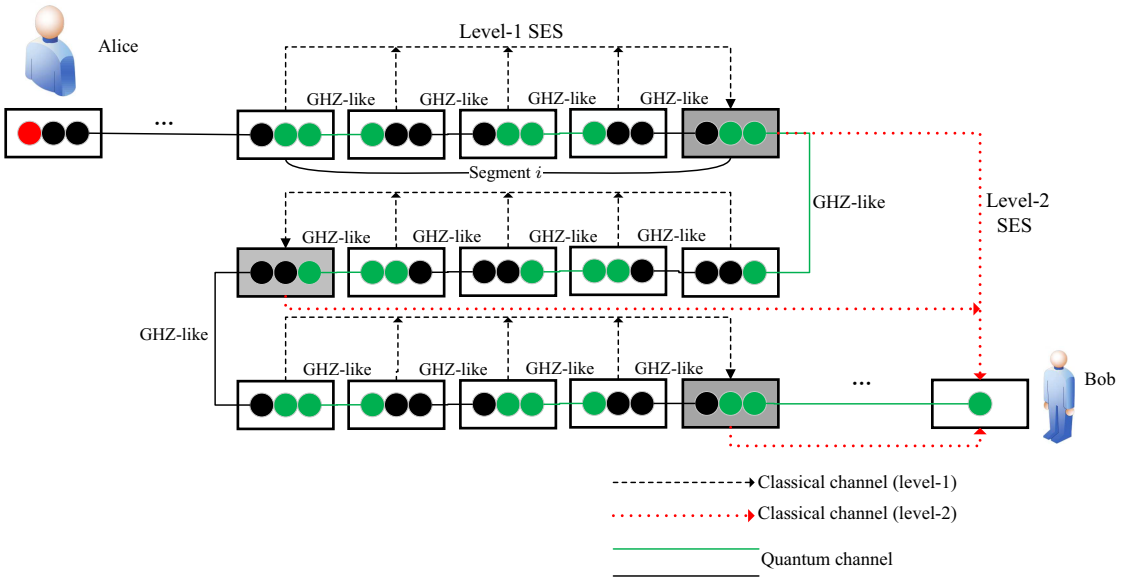


Fig. 4. Hierarchical simultaneous entanglement swapping.

Step 1 Entangled state preparation and distribution

This step is similar to the multi-hop QT described earlier, where all intermediate nodes can prepare any GHZ-like state. It is just divided into several parts.

Step 2 Level-one SES

The level-one SES involves simultaneously performing entanglement exchange within each segment and across all segments. Similar to previous multi-hop QT schemes, each node in the segment performs a measurement of the particles in its possession, then sends the measurement results and the type of the GHZ-like state to the end node of the segment through the classical channel. At the first segment, the source and end nodes can establish a GHZ state after the end nodes perform the corresponding operations according to Tables 4 and 5. At the same time, for each remaining segment, the nodes (including the end node of the first segment) in each segment perform simultaneous entanglement swapping (SES) independently. And all nodes of each segment (except the end node) use the GHZ-like states as the measurement basis on their own particles. Assume the measurement results of the intermediate nodes are $|\xi_{ijk}\rangle$ $(i,j,k=0,1)$, respectively, which can be encoded as three-bit ijk. Next, the measurement results codes and GHZ-like state types can be transmitted to the end node of each segment through the classical channel. Then, the end node of each segment will perform the appropriate Pauli operation to establish a GHZ-like state $|\xi_{000}\rangle$ between the two segments according to Tables 5 and 6. For all intermediate nodes of $|\xi_{000}\rangle$, the relationship between measurement results and Pauli operations is shown in Table 6. Here, R_{n_i}, R_{n_j} and R_{n_k} represent the value of the measurement of node$_n$. Namely, at the end of one level of SES, the end node and the source node of the first segment will establish the GHZ-like state,

while the neighboring end nodes of the remaining segments will establish the GHZ-like state $|\xi_{000}\rangle$.

Table 6. For all intermediate nodes of $|\xi_{000}\rangle$, the relationship between the measurement results and the operation of the rest of the nodes in the first-level SES except the first segment and end node. Here, each segment has q nodes.

Measurement results	Pauli operators
$\overline{\oplus_{n=1}^{n=q}R_{n_i}}\cdot\overline{\oplus_{n=1}^{n=q}R_{n_j}}\cdot\overline{\oplus_{n=1}^{n=q}R_{n_k}}=1$	I
$\oplus_{n=1}^{n=q}R_{n_i}\cdot\overline{\oplus_{n=1}^{n=q}R_{n_j}}\cdot\overline{\oplus_{n=1}^{n=q}R_{n_k}}=1$	X
$\overline{\oplus_{n=1}^{n=q}R_{n_i}}\cdot\overline{\oplus_{n=1}^{n=q}R_{n_j}}\cdot\oplus_{n=1}^{n=q}R_{n_k}=1$	Z
$\oplus_{n=1}^{n=q}R_{n_i}\cdot\overline{\oplus_{n=1}^{n=q}R_{n_j}}\cdot\oplus_{n=1}^{n=q}R_{n_k}=1$	ZX

Step 3 Level-two SES

The second level SES involves entanglement exchange between each segment. After completing the first-level SES, the entire quantum system also becomes the first-level SES, with the quantum channel entangled by composite states $|\xi_{000}\rangle$, as shown in Fig. 5. Therefore, each intermediate node is no longer required to send the type of the prepared GHZ-like state, but only the measurement results to the end node. Upon the completion of all processes, the end node calculates the unitary operation according to Table 3 and then reconstructs the target state.

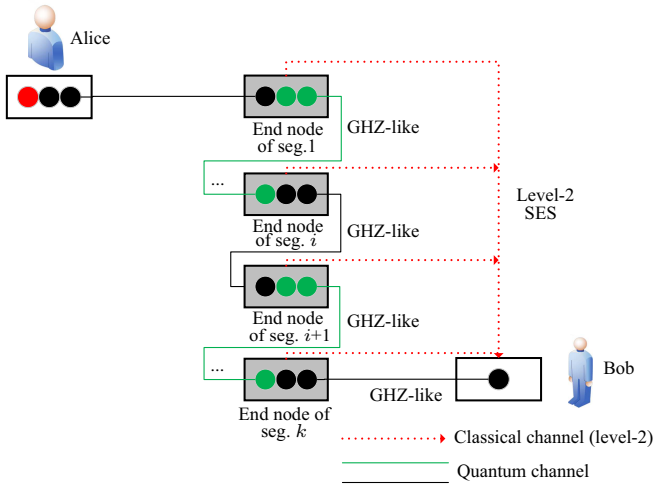


Fig. 5. Level-two SES.

For instance, assuming the communication in a quantum network is divided into five segments, the whole system can be represented as

$$|\Lambda\rangle = |\psi\rangle_0 \otimes |\xi_{ijk}\rangle_0 \otimes \cdots \otimes |\xi_{000}\rangle_{\text{end1}} \otimes \cdots \otimes |\xi_{000}\rangle_{\text{end2}} \otimes \cdots \otimes |\xi_{000}\rangle_{\text{end5}}. \quad (10)$$

Following level-one SES, the individual fragments become

$$|S_1\rangle = |\psi\rangle_0 \otimes |\xi_{000}\rangle_{\text{end1}},$$
$$|S_2\rangle = |\xi_{000}\rangle_{\text{end2}}\,|S_5\rangle = |\xi_{000}\rangle_{\text{end5}}. \quad (11)$$

Here, the 0, end1, ..., end5 represent the distribution of nodes, and $i, j, k \in (0,1)$. The whole system becomes

$$|\Lambda'\rangle = |\psi\rangle_0 \otimes |\xi_{000}\rangle_{\text{end1}} \otimes |\xi_{000}\rangle_{\text{end2}} \otimes |\xi_{000}\rangle_{\text{end3}} \otimes |\xi_{000}\rangle_{\text{end4}} \otimes |\xi_{000}\rangle_{\text{end5}}. \quad (12)$$

The level-two SES also transforms into a five-hop QT, and the end node can recover the target bits according to Table 4.

There is the requirement of transmitting measurements and GHZ-like state types to the end nodes of the segment in level-one SES, and the absence of the need to transmit GHZ-like state types in level-two SES. Thus, the HSES scheme significantly reduces the classical information cost.

5. Experimental realization of multi-hop QT in IBM QE

We have theoretically investigated and demonstrated the feasibility of multi-hop QT based on GHZ-like states. Various theoretical protocols have been validated on this platform.[20–31] Next, the scheme will be validated on the IBM QE platform. Now, take one-hop QT and two-hop QT implemented on a real quantum computer as an example. Assume that the initial state to be transmitted is $|\psi\rangle_0 = \frac{1}{\sqrt{2}}(|0\rangle + |1\rangle)_0$. The real quantum circuit diagram of one-hop QT and two-hop QT is shown in Fig. 6. The initial state preparation and quantum channel setup are depicted in the first half, followed by the channel entanglement and measurement in the second half. The quantum computer 'ibm_brisbane' was used to run the designed circuit ten times, with 8192 shots per run. The measurement results are recorded in Table 7. Figure 7 depicts the average of these measurement results, showing that the average error between the experimental and theoretical results for one-hop QT and two-hop QT is 0.0171 and 0.0083, respectively.

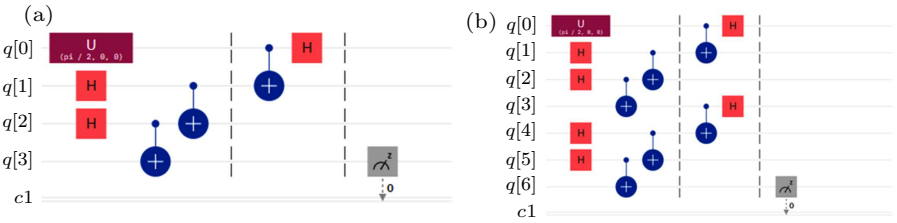


Fig. 6. The real quantum circuit diagrams of (a) one-hop QT and (b) two-hop QT.

Table 7. Ten times measurement results of one-hop QT and two-hop QT.

Runs	One-hop QT		Two-hop QT	
	Probability of $\|0\rangle$	Probability of $\|1\rangle$	Probability of $\|0\rangle$	Probability of $\|1\rangle$
1	0.4749	0.5251	0.4837	0.5163
2	0.4800	0.5200	0.4839	0.5161
3	0.4888	0.5112	0.4952	0.5048
4	0.4937	0.5063	0.5037	0.4963
5	0.4739	0.5261	0.4800	0.5200
6	0.4830	0.5170	0.4971	0.5029
7	0.4838	0.5162	0.4948	0.5052
8	0.4782	0.5218	0.4977	0.5023
9	0.4899	0.5101	0.4864	0.5136
10	0.4826	0.5174	0.4950	0.5050

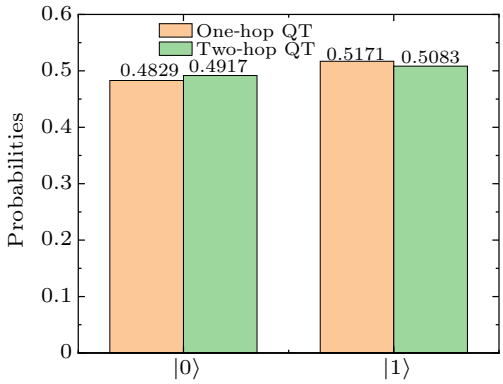


Fig. 7. The average of the measurement results of one-hop QT and two-hop QT.

Quantum state tomography is a common method for characterizing quantum states to characterize the performance of a scheme.[32–34] This includes the comparison of experimental and theoretical densities. For a given state $|\psi\rangle_0$, the theoretical density matrix ρ^{T} and the experimental density matrix ρ^{E} can be expressed as

$$|\rho^{\mathrm{T}}\rangle = |\psi\rangle\langle\psi|,$$

$$|\rho^{\mathrm{E}}\rangle = \frac{1}{2}[T_I(I) + T_X(X) + T_Y(Y) + T_Z(Z)], \tag{13}$$

where $T_i = S_i$ $(i = I, X, Y, Z)$ and S_i denotes the Stokes parameter. Here, $S_I = P_{|0I\rangle} + P_{|1I\rangle}$, $S_X = P_{|0X\rangle} - P_{|1X\rangle}$, $S_Y = P_{|0Y\rangle} - P_{|1Y\rangle}$ and $S_Z = P_{|0Z\rangle} - P_{|1Z\rangle}$, where $P_{|ki\rangle}$ denotes the probability of measuring $|k\rangle$ with i as the measurement basis (see Fig. 8). For the initial state $|\psi\rangle_0$, the theoretical density matrix is

$$|\rho^{\mathrm{T}}\rangle = \frac{1}{2}\begin{pmatrix} 1 & 1 \\ 1 & 1 \end{pmatrix}. \tag{14}$$

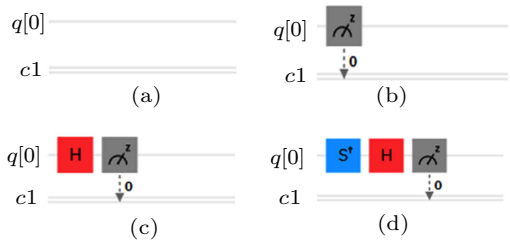


Fig. 8. Measurement in different bases: (a) I basis, (b) Z basis, (c) X basis, (d) Y basis.

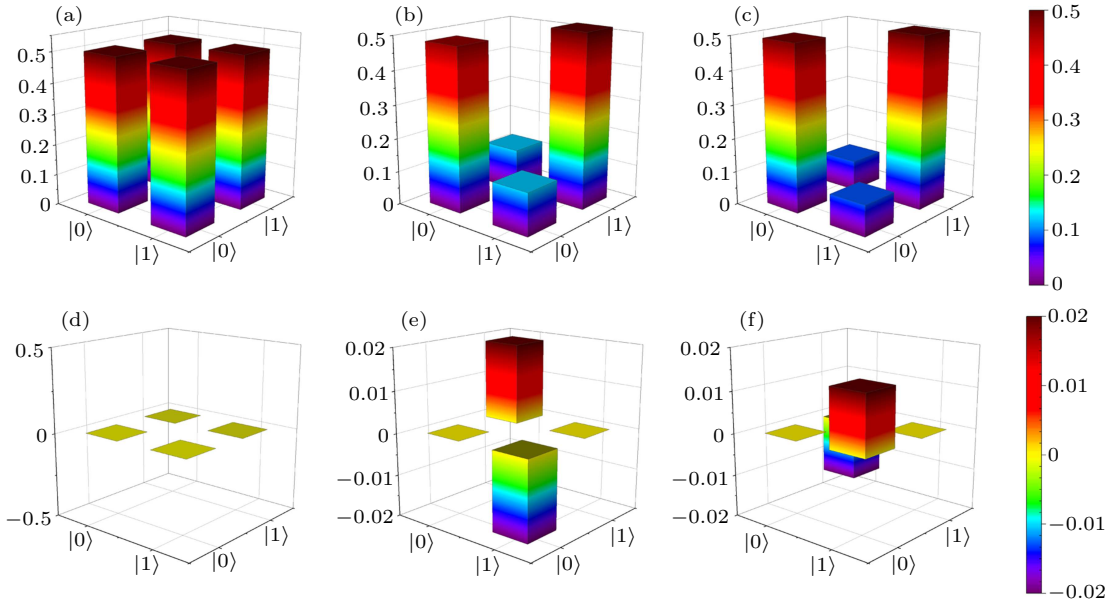


Fig. 9. Real and imaginary parts of experimental and theoretical density matrices for the teleportation of a single-qubit state in one-hop QT and two-hop QT, respectively. Here, (a), (b) and (c) are the real parts of the theoretical density matrix, the one-hop QT experimental density matrix and the two-hop QT experimental density matrix, respectively; (a), (b) and (c) are the imaginary parts of the theoretical density matrix, the one-hop QT experimental density matrix and the two-hop QT experimental density matrix, respectively.

Taking one-hop QT and two-hop QT as examples, their respective average experimental density matrices are calculated as follows (also shown in Fig. 9):

$$|\rho_1^{\mathrm{E}}\rangle = \begin{pmatrix} 0.4829 & 0.126 \\ 0.126 & 0.5171 \end{pmatrix} + \begin{pmatrix} 0 & -0.019 \\ 0.019 & 0 \end{pmatrix} \mathrm{i}, \quad (15)$$

$$|\rho_2^{\mathrm{E}}\rangle = \begin{pmatrix} 0.4917 & 0.091 \\ 0.091 & 0.5083 \end{pmatrix} + \begin{pmatrix} 0 & 0.014 \\ -0.014 & 0 \end{pmatrix} \mathrm{i}. \quad (16)$$

Fidelity is a measure of the overlap between the density matrix of the theoretical quantum state and the density matrix of the experimental quantum state, and a measure of how close the two quantum states are before and after transmission. When the fidelity is 1, this means that the output quantum state is identical to the target quantum state. The smaller the fidelity, the more quantum state information is lost. The fidelity is given by the following equation:

$$F(\rho^{\mathrm{T}}\rho^{\mathrm{E}}) = \mathrm{Tr}(\sqrt{\sqrt{\rho}^{\mathrm{T}}\rho^{\mathrm{E}}\sqrt{\rho}^{\mathrm{T}}}). \quad (17)$$

Here $F_1 = 89.12\%$ and $F_2 = 86.87\%$ are calculated to denote the fidelity of one-hop QT and two-hop QT, respectively. Then, the fidelity of the initial states $|\psi\rangle_0' = (\frac{1}{\sqrt{3}}|0\rangle + \sqrt{\frac{2}{3}}|1\rangle)_0$ and $|\psi\rangle_0'' = (\frac{1}{2}|0\rangle + \frac{\sqrt{3}}{2}|1\rangle)_0$ were computed through quantum state tomography to obtain $F_1' = 87.09\%$, $F_2' = 85.52\%$ and $F_1'' = 87.21\%$, $F_2'' = 84.61\%$, respectively. It can be shown that quantum states are transmitted with high fidelity in our scheme.

6. Effect on multi-hop QT by HSES with noise

The above experiments were conducted within an ideal environment. However, in the actual realization of QT, it is impossible to have an ideal environment (noiseless environment). When particles pass through a quantum channel, the entire quantum system may interact with its surroundings, potentially being disrupted by environmental noise. In this section, we discuss our protocol in four different noise environments, namely the phase-damping (P), amplitude-damping (D), phase-flip (F) and bit-flip (B) noises, which can be described in terms of the Kraus operator as follows:

$$E_0^P = \begin{pmatrix} \sqrt{1-p} & 0 \\ 0 & \sqrt{1-p} \end{pmatrix},$$

$$E_1^P = \begin{pmatrix} \sqrt{p} & 0 \\ 0 & 0 \end{pmatrix}, \quad E_2^P = \begin{pmatrix} 0 & 0 \\ 0 & \sqrt{p} \end{pmatrix}, \quad (18)$$

$$E_0^D = \begin{pmatrix} 1 & 0 \\ 0 & \sqrt{1-d} \end{pmatrix}, \quad E_1^D = \begin{pmatrix} 0 & \sqrt{d} \\ 0 & 0 \end{pmatrix}, \quad (19)$$

$$E_0^F = \begin{pmatrix} \sqrt{1-f} & 0 \\ 0 & \sqrt{1-f} \end{pmatrix}, \quad E_1^F = \begin{pmatrix} \sqrt{f} & 0 \\ 0 & -\sqrt{f} \end{pmatrix}, \quad (20)$$

$$E_0^B = \begin{pmatrix} \sqrt{1-b} & 0 \\ 0 & \sqrt{1-b} \end{pmatrix}, \quad E_1^B = \begin{pmatrix} 0 & \sqrt{b} \\ \sqrt{b} & 0 \end{pmatrix}, \quad (21)$$

where $p, d, f, b\,(0 \le p, d, f, b \le 1)$ are the corresponding four decoherence rates.

In Section 4, the source node wants to send the target quantum state $|\psi\rangle = (\alpha|0\rangle + \beta|1\rangle)$ to the target node through n nodes, and its density matrix can be expressed as $\rho_{\mathrm{in}} = |\psi\rangle\langle\psi|$. Assuming that node$_N$ ($N = 0, 1, \ldots, n-1$) is able to prepare a GHZ-class state $|\xi_{000}\rangle$, its density matrix can be expressed as $\rho_0^{C_{3N+1}C_{3N+2}C_{3N+3}} = |\xi_{000}\rangle\langle\xi_{000}|$. During the construction of a multi-hop QT system, node$_N$ will send its particle C_{3N+3} to the next neighboring node$_{N+1}$. Therefore, the particle C_{3N+3} will be acted upon by the Kraus operators. After the entanglement distribution, the pure states $\rho_0^{C_{3N+1}C_{3N+2}C_{3N+3}}$ are converted to mixed states, which can be written as $\rho_1^{C_{3N+1}C_{3N+2}C_{3N+3}} = \sum_l E_l^{kC_{3N+3}} \rho_0^{C_{3N+1}C_{3N+2}C_{3N+3}} (E_l^{kC_{3N+3}})^\dagger (k \in \{P, D, F, B\})$, $l \in \{0, 1, 2\}$. Assuming that the whole quantum channel is in the same kind of noise, the density matrix of the whole quantum system becomes

$$\rho_{\mathrm{c}}^n = \rho_{\mathrm{in}} \otimes_{N=0}^{n-1} \rho_1^{C_{3N+1}C_{3N+2}C_{3N+3}}. \quad (22)$$

From the description of level-one in Section 4, assuming that there are q nodes in each segment, the output state of the whole system, after the measurements and operations, becomes

$$\rho_{\mathrm{L}_1} = U\left(\mathrm{Tr}\left[\frac{(\otimes_{i=1}^{n/q}\otimes_{j=1}^{q-1} M_{ij})\rho_{\mathrm{c}}^n(\otimes_{i=1}^{n/q}\otimes_{j=1}^{q-1} M_{ij})^\dagger}{\mathrm{Tr}\{(\otimes_{i=1}^{n/q}\otimes_{j=1}^{q-1} M_{ij})^\dagger(\otimes_{i=1}^{n/q}\otimes_{j=1}^{q-1} M_{ij})\rho_{\mathrm{c}}^n\}}\right]\right)U^\dagger, \quad (23)$$

where M_{ij} denotes the measurement result of the particle owned by the jth node in the ith segment. After completing level-two, the output state of the reconfigured quantum state of the target node$_{n-1}$ can be expressed as

$$\rho_{\mathrm{out}} = U\left(\mathrm{Tr}\left[\frac{(\otimes_{i=1}^{n/q} M_i)\rho_{\mathrm{L}_1}(\otimes_{i=1}^{n/q} M_i)^\dagger}{\mathrm{Tr}\{(\otimes_{i=1}^{n/q} M_i)^\dagger(\otimes_{i=1}^{n/q} M_i)\rho_{\mathrm{L}_1}\}}\right]\right)U^\dagger. \quad (24)$$

Thus, the density matrix of the output states in each of the four noise environments can be expressed as

$$\begin{aligned}
\rho_{\mathrm{out}}^P &= (1-p)^n(\alpha^2|0\rangle\langle 0| + \alpha\beta|0\rangle\langle 1| \\
&\quad + \alpha\beta|1\rangle\langle 0| + \beta^2|1\rangle\langle 1|) + p^n\alpha^2|0\rangle\langle 0|, \\
\rho_{\mathrm{out}}^D &= \alpha^2|0\rangle\langle 0| + \sqrt{1-d}\alpha\beta|0\rangle\langle 1| \\
&\quad + \sqrt{1-d}\alpha\beta|1\rangle\langle 0| + (1-d)\beta^2|1\rangle\langle 1|, \\
\rho_{\mathrm{out}}^F &= (1-f)^n(\alpha^2|0\rangle\langle 0| + \alpha\beta|0\rangle\langle 1| \\
&\quad + \alpha\beta|1\rangle\langle 0| + \beta^2|1\rangle\langle 1|) + f^n(\alpha^2|0\rangle\langle 0| \\
&\quad - \alpha\beta|0\rangle\langle 1| - \alpha\beta|1\rangle\langle 0| + \beta^2|1\rangle\langle 1|), \\
\rho_{\mathrm{out}}^B &= (1-b)^n(\alpha^2|0\rangle\langle 0| + \alpha\beta|0\rangle\langle 1| \\
&\quad + \alpha\beta|1\rangle\langle 0| + \beta^2|1\rangle\langle 1|) + b^n(\alpha^2|1\rangle\langle 1| \\
&\quad + \alpha\beta|1\rangle\langle 0| + \alpha\beta|0\rangle\langle 1| + \beta^2|0\rangle\langle 0|). \quad (25)
\end{aligned}$$

The quantum system will be disturbed by external noise, which causes the coherence property of the quantum system to decrease, thus making the difference between the two quantum

states before and after transmission. In quantum information theory, the fidelity is generally used to measure the proximity between two quantum states before and after transmission, calculated as

$$F = |\langle\psi|\rho_{\text{out}}|\psi\rangle|. \tag{26}$$

The F denotes the similarity between the output quantum state and the target quantum state, taking values from 0 to 1. When the fidelity is 1, this means that the output quantum state is identical to the target quantum state. The lower the fidelity, the more information of the quantum state is lost. The fidelity of the protocol under four different noises is calculated as

$$\begin{aligned} F^P &= (1-p)^n(\alpha^2+\beta^2)^2 + p^n\alpha^4, \\ F^D &= \alpha^4 + \sqrt{1-d}2\alpha^2\beta^2 + (1-d)\beta^4, \\ F^F &= (1-f)^n(\alpha^2+\beta^2)^2 + f^n(\alpha^2-\beta^2)^2, \\ F^B &= (1-b)^n(\alpha^2+\beta^2)^2 + 4b^n\alpha^2\beta^2. \end{aligned} \tag{27}$$

From the above calculations, it is found that in the phase-damping (P), phase-flip (F) and bit-flip (B) noise, the fidelity of the output state depends on the coefficients of the initial state, decoherence rate and number of nodes. However, in the amplitude-damping (D) noise, the fidelity of the output state depends only on the coefficients of the initial state and the decoherence rate. To study the trend of fidelity with decoherence rate and number of nodes, we assume that the coefficients of the target state are $\alpha = 1/\sqrt{2}$ and $\beta = 1/\sqrt{2}$. The trend of fidelity under four types of noise is given in Fig. 10.

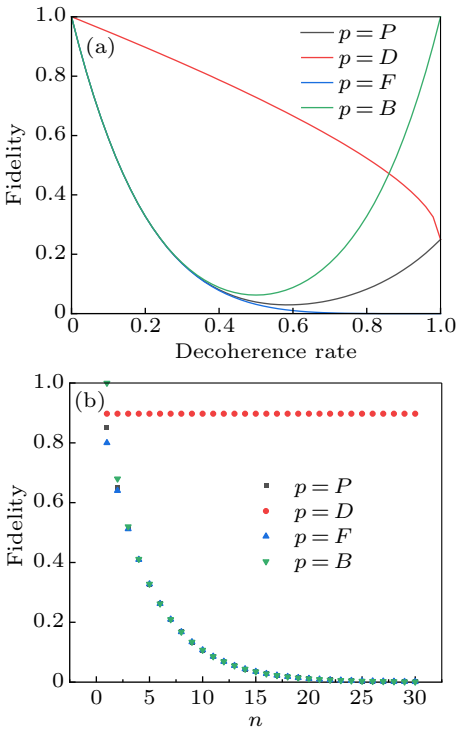


Fig. 10. Comparison of the fidelity under the influence of four types of noise (P, D, F, B). (a) The fidelity varies with decoherence rate at $n = 5$. (b) The fidelity varies with node n at decoherence rate $(p, d, f, b) = 0.8$.

In Fig. 10(a), initially, the fidelity decreases with increasing decoherence rate for all four noise environments, and it is clear that the fidelity is subject to the slow decrease in amplitude-damping (D) noise and the fastest decrease in phase-flip (F) noise. As the decoherence rate increases, the fidelity of bit-flip (B) noise gradually recovers to a symmetric shape, while phase-damping (P) noise increases slowly. This shows that the output state fidelity does not necessarily decrease with increasing decoherence, meaning that in some noisy environments, stronger noise can result in higher multi-hop QT efficiency. In Fig. 10(b), it is clear that the fidelity of the subject amplitude-damping (D) noise does not change with n, while the fidelity under all the other three noises gradually decreases with the increase in n. Namely, in some noisy environments, the output state fidelity does not necessarily decrease as the number of intermediate nodes increases.

7. Communication delays and classical resource consumption

7.1. Communication delays

In quantum teleportation, communication delay is inevitable. This delay is primarily influenced by factors such as the time required for classical communication, the duration of quantum state processing (including measurement and unitary transformation), etc. For a multi-hop QT protocol with general simultaneous measurements (SES), the communication delay of classical information depends on the maximum delay from each intermediate node to the end node. The HSES scheme is introduced. In the level-one SES, the communication delay of classical messages depends on the maximum delay from each intermediate node of a segment to its end node. In the level-two SES, the delay depends on the maximum delay from the end node of each segment to the end node. Therefore, the total delay D of our scheme is

$$\begin{aligned} D \;=\; & H_{\max 1}(D_{\text{c}} + D_{\text{pro}} + L_{\text{mt}}/R) \\ & + H_{\max 2}(D_{\text{c}} + D_{\text{pro}} + L_{\text{m}}/R) + 2D_{\text{m}} + 2D_{\text{u}}, \end{aligned} \tag{28}$$

where D_{m} represents the time required for measurement, D_{u} indicates the duration of unitary transformation, D_{c} denotes the time taken for single-hop classical information communication, D_{pro} is the average processing time for a classical packet, $H_{\max 1}$ denotes the maximum number of classical hops from the first intermediate node to the end nodes across all segments and $H_{\max 2}$ symbolizes the maximum number of classical hops from each end node to Bob. L_{mt} is the total length of the classical packet that contains the information about the GHZ-like state type and three-bit measurement result, and L_{m} represents the length of the classical packet that contains the three-bit measurement result. R is the transmission rate of the classical information.

Now, assume the propagation rate of photon in the air is 2.996×10^5 km/s. $D_{\rm m}$, $D_{\rm u}$ and R are 100 ns, 50 ns and 100 Mbit/s, respectively.[19] In ethernet frames, the shortest packet length is 512 bits, so the classical information of GHZ-like state and three-bit measurement results can be carried by a standard packet, namely $L_{\rm mt}$, and $L_{\rm m}$ can be taken at 512 bits. Assuming that the distance of a quantum hop is 10 km, the comparison of the communication delay of the present protocol with the traditional SES in Section 2 is shown in Fig. 11(a), where it can be seen that the communication delay of the present protocol is lower than that of the traditional SES. In addition, the delay of this protocol is higher when the number of nodes in each segment is greater.

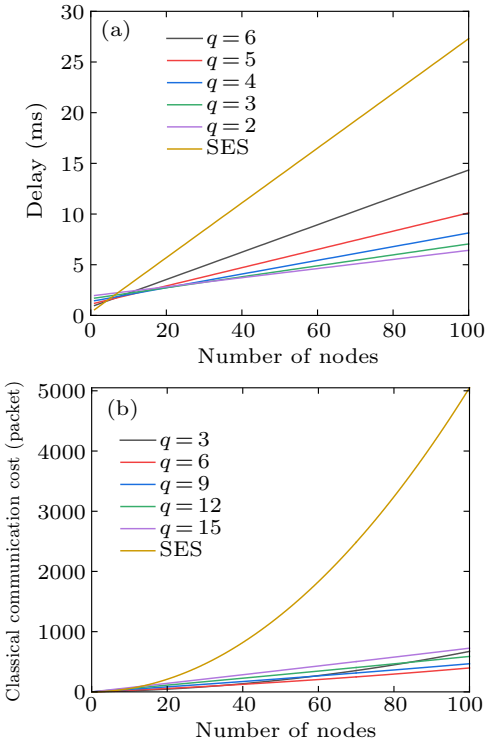


Fig. 11. Comparison between the traditional SES scheme and this protocol (with a different number of nodes in each segment) in terms of both delay and classical resource consumption. (a) Comparison with traditional SES scheme in terms of delay when the nodes in this protocol segment are 2–6, respectively. (b) Comparison of classical resource consumption with traditional SES scheme when the nodes in this protocol segment are 3, 6, 9, 12 and 15, respectively.

7.2. Classical resource consumption

In general, in a simultaneous measurement protocol (SES), each intermediate node is required to send the measurement result and the type of entangled state to the end node via the classical channel, resulting in significant classical resource wastage. In contrast, the proposed scheme initially follows a communication pattern similar to that of SES, but in the second layer, each segmented end node only needs to send the measurement results to the end node over the classical channel without sending the types of entangled states. This approach significantly reduces the consumption of classical resources. Since classical information needs to be encapsulated in ethernet frames, we use packets as the unit of classical resource consumption. The equation for classical resource consumption is given by

$$C = \sum_{i=1}^{S} \sum_{j=1}^{N_{Si}-1} L_{\rm mt} H_{ij}^{S} + \sum_{i=1}^{S} L_{\rm m} H_i^{\rm d}, \tag{29}$$

where S represents the division of N nodes into S sections, N_{Si} indicates the number of nodes in the ith section, H_{ij}^{S} denotes the number of hops from the ith node in the ith section to the end node in the ith section and $H_i^{\rm d}$ represents the number of hops from the end node in the ith section to the end node.

The classical resource consumption comparison of this protocol with the traditional SES in Section 2 is shown in Fig. 11(b), which shows that the classical resource consumption of this protocol is much smaller than that of the classical resource consumption of the traditional SES scheme. It is interesting to note that the more nodes in each segment, the less classical resource consumption. As shown in Fig. 11(b), when the number of nodes per part is six (compared with $q = 3$, 9, 12, 15) the classical resource consumption is the least. In other words, for different numbers of nodes, choosing the appropriate segmentation method can achieve the optimal classical resource consumption.

8. Conclusion

This paper introduces a multi-hop QT scheme based on the HSES using GHZ-like states. First, the schemes of one-hop QT and two-hop QT are described in detail and then extended to multi-hop QT. The relationship between the measurement results and the unitary operation of the target node for recovering the target state is derived. A generalized logic algebraic expression is used to determine the recovery Pauli operator of the target node for recovering a single bit. Considering also the practical situation where the types of GHZ-like states entangled in a quantum channel are different, the modified unitary operation of the target node is derived based on the number of different GHZ-like states. Next, we introduce a multi-hop QT protocol based on the HSES protocol, which involves simultaneous entanglement swapping within and between all segments. Since the intermediate nodes at the level-two of SES only need to send measurement results to the end nodes, the consumption of classical resources is drastically reduced.

In addition, in conjunction with the practical situation, we analyze the impact of four different noise environments (phase-damping, amplitude-damping, phase-flip and bit-flip) on our scheme. The results show that the fidelity is related to the amplitude parameter, decoherence rate and number of nodes, as shown in Fig. 10. By analyzing the results and the

curve trend of Fig. 10, we can choose a suitable noise environment to prepare the quantum channel and transmit the target state in conjunction with the actual situation, which can effectively reduce the information loss in the transmission process.

The proposed scheme offers several advantages. First, it does not require all intermediate nodes to share the same type of GHZ-like state, which is practical because it is unrealistic for all nodes in a real quantum network to share only one type of entangled state. Second, the IBM QE platform is used to simulate one-hop QT and two-hop QT cases. Analyzing the experimental results with quantum state tomography demonstrates that the scheme achieves good fidelity. Finally, the proposed scheme exhibits lower classical resource consumption compared to general simultaneous entanglement switching multi-hop QT protocols.

Acknowledgements

Project supported by the Open Fund of Anhui Key Laboratory of Mine Intelligent Equipment and Technology (Grant No. ZKSYS202204), the Talent Introduction Fund of Anhui University of Science and Technology (Grant No. 2021yjrc34), and the Scientific Research Fund of Anhui Provincial Education Department (Grant No. KJ2020A0301).

References

[1] Bennett C H, Brassard G, Crépeau C, Jozsa R, Peres A and Wootters W K 1993 *Phys. Rev. Lett.* **70** 1895
[2] Bouwmeester D, Pan J W, Mattle K, Eibl M, Weinfurter H and Zeilinger A 1997 *Nature* **390** 575
[3] Gisin N and Bechmann-Pasquinucci H 1998 *Phys. Lett. A* **246** 1
[4] Kiktenko E O, Popov A A and Fedorov A K 2016 *Phys. Rev. A* **93** 062305
[5] Verma V 2020 *IEEE Commun. Lett.* **25** 936
[6] Du Z, Li X and Liu X 2020 *Int. J. Theor. Phys.* **59** 622
[7] Sk R, Dash T and Panigrahi P K 2021 *IET Quantum Commun.* **2** 122
[8] Verma V 2020 *Mod. Phys. Lett. A* **35** 2050333
[9] Dong L, Xiu X M, Gao Y J, Ren Y P and Liu H W 2011 *Opt. Commun.* **284** 905
[10] Tsai C W and Hwang T 2010 *Int. J. Theor. Phys.* **49** 1969
[11] Joo J, Park Y J, Oh S and Kim J 2003 *New J. Phys.* **5** 136
[12] Briegel H J, Dür W, Cirac J I and Zoller P 1998 *Phys. Rev. Lett.* **81** 5932
[13] Cheng S T, Wang C Y and Tao M H 2005 *IEEE J. Sel. Areas Commun.* **23** 1424
[14] Wang K, Yu X T, Lu S L and Gong Y X 2014 *Phys. Rev. A* **89** 022329
[15] Cai R, Yu X T and Zhang Z C 2018 *Int. J. Theor. Phys.* **57** 1723
[16] Chen N, Shuai S, Yan B, Xu N and Pei C 2020 *IEEE Access* **8** 52052
[17] Zhang Z and Sang Y 2023 *Quantum Inf. Process.* **22** 201
[18] Wu F, Tang L, Bai M Q and Mo Z W 2023 *Phys. Stat. Mech. Its Appl.* **625** 129022
[19] Yang G, Xing L, Nie M, Liu Y H and Zhang M L 2021 *Chin. Phys. B* **30** 030301
[20] Gayathri Devi S, Manjula Gandhi S, Chandia S and Boobalaragavan P 2023 Exploring IBM Quantum Experience *Quantum Computing: A Shift from Bits to Qubits* Studies in Computational Intelligence Vol. 1085, ed R Pandey, N Srivastava, N K Singh and K Tyagi (Singapore: Springer Nature Singapore) pp. 265–82
[21] Sisodia M 2020 *Quantum Inf. Process.* **19** 215
[22] Wei S J, Xin T and Long G L 2018 *Sci. China Phys. Mech. Astron.* **61** 70311
[23] Kumar A, Haddadi S, Pourkarimi M R, Behera B K and Panigrahi P K 2020 *Sci. Rep.* **10** 13608
[24] Sisodia M, Shukla A and Pathak A 2017 *Phys. Lett. A* **381** 3860
[25] Majumder A, Mohapatra S and Kumar A 2017 arXiv:1707.07460v3 [quant-ph]
[26] Alsina D and Latorre J I 2016 *Phys. Rev. A* **94** 012314
[27] Harper R and Flammia S T 2019 *Phys. Rev. Lett.* **122** 080504
[28] Dharkar V and Kumar S 2024 2024 *International Conference on Computing, Networking and Communications (ICNC)* (Big Island, HI, USA: IEEE) pp. 11–5
[29] Kim M, Hwang M R, Jung E and Park D 2023 *Quantum Inf. Process.* **22** 176
[30] Jiang Y, Li D, Zhu Y, Hua X, Fu Y, Zhou J, Yang X and Tan Y 2024 *Int. J. Theor. Phys.* **63** 86
[31] Huffman E and Mizel A 2017 *Phys. Rev. A* **95** 032131
[32] Vishnu P K, Joy D, Behera B K and Panigrahi P K 2018 *Quantum Inf. Process.* **17** 274
[33] Yang G, Yang R, Gong Y X and Zhu S N 2023 *Chin. Phys. B* **32** 110306
[34] Li J, Zhu J L, Gao J, Pang Z G and Wang Q 2022 *Chin. Phys. Lett.* **39** 070303